Fatigue damage characteristics of a flexible cylinder under concomitant excitation of time-varying axial tension and VIV

Yan Lu [a,b], Zhenchao Yu [b], Yexuan Ma [c], Zhanxiang Liu [b], Wanhai Xu [a,b,*]

[a] *State Key Laboratory of Hydraulic Engineering Simulation and Safety, Tianjin University, Tianjin, 300350, China*
[b] *School of Civil Engineering, Tianjin University, Tianjin, 300350, China*
[c] *Institute of Mechanics, Chinese Academy of Sciences, Beijing, 100190, China*

ARTICLE INFO

ABSTRACT

Flexible cylindrical structures are susceptible to the concomitant excitation of vortex-induced vibration (VIV) and time-varying axial tension in offshore engineering. The structural instability caused by the simultaneous excitation can lead to severe fatigue damage, threatening the safe application of cylindrical structures. In this paper, experimental research was conducted on a long flexible cylinder with an aspect ratio of $L/D = 350$ to investigate its fatigue characteristics under the concomitant excitation. The reduced velocity V_r ranged from 1.34 to 26.71. The axial tension excitation was characterized by three axial tension amplitude ratios $T_v/T_c = 0.1–0.3$ (where T_v is the tension amplitude and T_c is the constant tension) and six axial tension frequency ratios $f_v/f_1 = 0.5–4.0$ (where f_v is the tension frequency and f_1 is the fundamental frequency of the cylinder). The $S–N$ curve method and the linear accumulative damage theory were employed to estimate the fatigue damage. The effects of reduced velocity, excitation amplitude and excitation frequency on the fatigue damage characteristics were discussed in terms of the fatigue damage distribution and maximum fatigue damage. The effect of the tension excitation on the fatigue damage is more pronounced at low reduced velocities ($V_r \leq 5.34$) when the VIV is not excited, since the axial tension can excite the mode vibration. The fatigue damage area and maximum fatigue damage are significantly enhanced with the increase of the tension amplitude ratio and frequency ratio due to the occurrence of higher-order mode vibrations. The effect of axial tension excitation on the fatigue damage of the cylinder is more pronounced in the in-line (IL) direction than in the cross-flow (CF) direction. However, for a small amplitude ratio ($T_v/T_c = 0.1$), the tension excitation is only noticeable with a large frequency ratio ($f_v/f_1 = 4.0$). On the other hand, as the reduced velocity increases, the VIV of the cylinder is excited and dominates the fatigue characteristics. The accumulative fatigue damage distribution is aggravated with the increase of reduced velocity. The time-varying axial tension has a negligible effect on the fatigue damage distribution features and the maximum fatigue damage values of the cylinder. Nevertheless, under certain circumstances, the axial tension excitation can slightly alleviate the fatigue damage in some regions along the cylinder.

1. Introduction

As the demand for the exploitation of offshore oil and gas resources is increasing continuously, long slender structures have been extensively used and concerned in recent years, such as top-tensioned risers (TTRs), steel catenary risers (SCRs), and tethers of tension leg platforms (TLPs). Due to the complicated marine environment, slender cylindrical structures are usually subjected to multiple loads during their service. Among these loads, the wave can cause the heave motion of the floating platforms, generating the axial tension fluctuation of the cylinder (Chen et al., 2015), while the flow can cause the periodic vortex shedding and pressure variation around the cylinder, resulting in its vortex-induced vibrations (VIVs). Therefore, the perennial axial tension parametric excitation and VIV excitation are the primary threats for serious fatigue damage of the slender cylindrical structure (Song et al., 2016), especially under the combined excitation (Drumond et al., 2018; Yang and Xiao, 2014).

Vortex-induced vibration (VIV) is a complicated fluid-structure interaction between the flexible structure and its vortex shedding, causing a serious concern for structural integrity and fatigue life (Triantafyllou et al., 2016). Heretofore, substantial research has been conducted on the VIV characteristics of the flexible cylinders from the

perspective of response (Xu et al., 2018), vortex shedding mode (Li and Ishihara, 2021), hydrodynamic features (Xu et al., 2017), and fatigue damage (Trim et al., 2005). Different from the rigid cylinders, the long slender cylinders have more complicated VIV responses, such as multi-mode response and high-order harmonic characteristics (Fan et al., 2015; Liu et al., 2020; Xu et al., 2020). A traveling-wave-dominated response pattern is also observed with the increase in towing speed (Ge et al., 2009). Trim et al. (2005) experimentally studied the VIV fatigue damage characteristics of the flexible cylinders with an aspect ratio $L/D = 1400$ (where L denotes the cylinder's length and D denotes the diameter) in the in-line (IL) and cross-flow (CF) directions and examined the fatigue damage suppression efficiency of different helical strakes. Besides, Resvanis et al. (2015) proposed a ramp test method with continuously varying towing speeds to obtain more VIV response results, and based on which the authors clarified the effect of the towing speed on the VIV response of a flexible cylinder. As the VIV characteristics of the cylinder are increasingly studied, it is possible to predict the VIV response and fatigue damage based on the mechanism. For example, Mentzelopoulos et al. (2022) provided a data-driven VIV response prediction method. Lu et al. (2022) proposed a VIV fatigue damage prediction method based on RBF neural network.

Furthermore, researchers have also focused on the response and fatigue damage of the immersed cylinder excited by the axial tension. This periodical excitation generated by the vertical motion of the platform affects the modal properties of the cylinders. Gu et al. (2016) found that the vibration amplitude of the cylinder is considerably reduced under the axial-tension excitation, which is possibly due to the variation of the cylinder's stiffness (Liu et al., 2020). Similarly, Sanaati and Kato (2012) also revealed that the application of the axial tension can decrease the lock-in bandwidth of the VIV and reduce the vibration amplitude. Wang et al. (2014) performed a truncated SCR model test to investigate the influence of amplitude and period on the heave-induced VIV response and fatigue damage of a cylinder. It was suggested that the fatigue damage is more sensitive to the amplitude than to the period and that the maximum fatigue damage position changes due to traveling wave and wave reflection phenomena. A time-domain numerical analysis procedure was proposed to investigate the fatigue damage of the cylinders under multi-degree-of-freedom excitation (Yuan et al., 2021). It was found that the cylinder manifests strong nonlinearity under multi-degree-of-freedom motion. The axial heave excitation has a weaker effect on the cylinder's fatigue damage than other excitations.

Under the coupling excitation of VIV and time-varying axial tension, the cylinder exhibits more complicated response characteristics due to Mathieu's instability and sustains aggravated fatigue damage. Yang and Xiao (2014) derived the non-autonomous motion governing equation, based on which they studied the dynamic response and instability of TTR systems under different excitations. It was found that the time-varying axial-tension excitation becomes the predominance under extreme conditions. Zhang et al. (2022) obtained the instability region of the Mathieu equation through the differential quadrature method and the Floquet theory. Wang et al. (2015) established the mechanical model for dynamic response analysis and calculated the Mathieu instability region using the perturbation method. In addition, a single-mode nonlinear reduced-order model (ROM) (Franzini et al., 2016) and a three-order reduced-order model (Franzini and Mazzilli, 2016) were proposed for the flexible cylinder subjected to axially harmonic parametric excitation through theoretical analysis. The difference between the two ROMs is related to the dominant response frequency in the amplitude spectra. These authors found that the structural response is dominated by the first sinusoidal mode due to the principal Mathieu's instability of the first mode. Zhang et al. (2018) studied the dynamic responses of a riser subjected to axially harmonic tension by means of the finite element method, finding that increasing the tension amplitude can enhance the stress of the cylinder while increasing the tension frequency can broaden the resonance region. The displacement response of

the cylinder is considerable when the excitation frequency is approximate twice the values of the fundamental frequency due to Mathieu's instability.

However, few experimental studies have been done on the response characteristics of the cylinder. Franzini et al. (2018) conducted a model experiment on a flexible cylinder under coupling VIV and axial top motion excitation. The reduced velocity V_r ranged from 1.6 to 15.0, the axial amplitude ratio A_{t/L_0} was 0.01 (where $L0$ is the length of the cylinder) and the excitation frequency ratio f_v/f_1 (where f_1 is the 1st-order natural frequency) was 2.0 and 3.0. These authors concluded that the axial top-motion can excite larger vibration amplitude and generate motion trajectory disorder. Moreover, amplitude modulations and multi-dominant-frequency response were observed under concomitant excitation. Likewise, another experiment on an immersed cylinder was performed considering the modal and spectral analysis and Mathieu instability modeling (Franzini et al., 2015). The results demonstrated that as the excitation frequency ratio $f_v/f_{N,1}$ increases from 1/3 to 3/1, the predominant response shifts from the first and second Eigenmodes to the third Eigenmode, indicating that the Mathieu's instability occurs in more than one Eigenmode. Recently, Ma et al. (2020) performed model tests to investigate the dynamic characteristics of a flexible-mounted cylinder under combined parametric excitation and VIV. It is found that the effect of axial tension frequency is enhanced with the increase in the axial tension amplitude. The low-frequency axial tension excitation can cause the cylinder an earlier entrance to higher-order modes and a wider mode resonance region. Amplitude modulation becomes considerable with the axial-tension frequency increasing. However, experiments on the cylinder with helical strakes indicated that the suppression efficiency of the straked cylinder can be significantly reduced due to the parametric axial tension excitation (Ma et al., 2021). The in-line (IL) displacements of the strake cylinder are enhanced under most tested amplitude ratios and frequency ratios due to the axial tension excitation.

As discussed above, the dynamic responses and fatigue performance of the cylinder under VIV excitation or parametric excitation have been extensively studied. However, most of the previous research investigating the influence of the combined parametric and VIV excitations mainly used theoretical analysis or numerical simulation, but few have explored the dynamic characteristics based on model experiments. Additionally, there is still a lack of studies focusing on the fatigue characteristics of the cylinder under simultaneous VIV excitation and axial tension excitation. Therefore, this paper endeavors to analyze the fatigue damage characteristics of a flexible cylinder under the concomitant excitement of VIV and time-varying axial tension through model experiments (Ma et al., 2020). Based on the rainflow counting method and S–N curve method, the spatiotemporal strain and fatigue damage distribution characteristics of the cylinder are examined. The fatigue damage of the tested cylinders is compared with that of the cylinder subjected to constant axial tension. Overall, new contributions of the current work include: (1) substantial model experiments considering various VIV and time-varying axial-tension excitationshave been conducted to systematically discuss the fatigue damage characteristics of a flexible cylinder, and (2) the effects of parametric excitation and VIV excitation on the fatigue characteristics have been further discussed through comparative analysis.

The remained of the paper is structured as follows. In Section 2, the experimental design and data process methodology are briefly introduced. In Section 3, the experimental results are presented and discussed in detail in terms of the strain distribution, fatigue damage distribution, and maximum fatigue damage. Eventually, in Section 4, some attractive conclusions are issued.

2. Methodology

2.1. Experimental design

The cylinder model tests were performed in a towing water tank in

the State Key Laboratory of Hydraulic Engineering Simulation and Safety at Tianjin University. The schematic diagram of the experimental setup is illustrated in Fig. 1(a). The experimental apparatus comprises the towing system, the axial-tension excitation system, and the supporting structures. The flexible cylinder model was simply supported at the guide plate through the universal joints. The steel wire with a tensioner was connected at the end of the cylinder model, applying the initial tension of 400 N. The VIV excitation is achieved through the uniform motion of the carriage along the track. The uniform motion of the carriage represents the constant velocity U of the oncoming flow towards the cylinder model, i.e., the reduced velocity of the flow is $V_r = U/(D \cdot f_1)$ (where D is the external diameter of the cylinder and f_1 is the fundamental frequency of the cylinder model). Additionally, the time-varying tension excitation is realized through the change of the working frequency f_v and eccentric distance A_v of the eccentric electric motor, which was monitored by the load cell on the apparatus. Consequently, the time-varying axial tension applied on the cylinder is $T_v \cdot \cos(2\pi \cdot f_v \cdot t)$ (where $T_v = k_s \cdot A_v$, among which k_s is the spring stiffness).

The cylinder model with a length of 5.60 m consists of an external silicone tube and an internal copper pipe. Seven measurement points (G1-G7) were evenly distributed along the cylinder, see Fig. 1(b). At each measurement point, four gauges were attached to the inner copper pipe to collect the in-line (IL) and cross-flow (CF) bending strains during the experiment, as shown in Fig. 1(c). Similar cylinder models have also been also adopted in experimental studies of the flow-induced vibration response and hydrodynamic characteristics of two, three, and four cylindrical structures (Ma et al., 2019; Xu et al., 2021a, 2022).

In addition, the flexible cylinder with an axial pretension of 400 N in this study has a damping ratio ζ_w of 0.032, obtained from the free decay tests in water (Ma et al., 2020). The damping ratio can be calculated as (Han et al., 2018a,b),

$$\zeta_w = \frac{\ln\left(Y_i / Y_{i+j}\right)}{2j\pi} \tag{1}$$

where Y_i is the strain response amplitude of the i-th cycle and Y_{i+j} is the strain response amplitude of the $(i+j)$-th cycle. Structural damping can

affect the VIV response of the tensioned cylinder (Vandiver et al., 2018). In this study, the damping ratio of the cylinder is relatively low, and the resonant response amplitude may depend on the limit cycle behaviour under lock-in conditions.

The geometric and mechanical parameters of the cylinder model are itemized in Table 1.

Regarding the VIV excitation, the oncoming flow velocity U was selected to be 0.05 m/s ~ 1.00 m/s (with an interval of 0.05 m/s), corresponding to the Reynolds numbers $Re = 800$–16000. Moreover, concerning the time-varying excitation, the axial-tension amplitude ratio T_v/T_c (where T_v is the excitation tension amplitude) was designed as 0.1, 0.2, and 0.3 and the frequency ratio f_v/f_1 (where f_v is the excitation frequency) was set as 0.5, 1.0, 1.5, 2.0, 3.0, and 4.0. Totally 18 different time-varying excitation cases were tested. However, for the case of $f_v/f_1 = 4.0$ (i.e., $f_v = 9.36$ Hz), the rotation speed of the electric motor exceeds the rated speed. To guarantee the safety of the experiments, the oncoming flow velocity ranged from 0.10 m/s to 1.00 m/s with an interval of 0.10 m/s in this case, corresponding to the reduced velocity V_r varying from 2.67 to 26.71. The specific test matrix is listed in Table 2. A more elaborate analysis on the experimental case selection can be referred to in the previous research (Ma et al., 2020). During the experiment, the IL and CF strains at G1-G7 were acquired with a sampling time of 50 s and a sampling frequency of 100 Hz. To eliminate the water flow effect, the interlude between two adjacent experimental

Table 1
Parameters of the flexible cylinder model.

Parameter	Values
Length, L (m)	5.60
Diameter, D (m)	0.016
Aspect ratio, L/D	350
Bending stiffness, EI (N•m^2)	17.45
Axial stiffness, EA (N)	2.793×10^6
Initial axial tension, T_c (N)	400
Mass ratio, m^*	1.90
Natural frequency, f_1 (Hz)	2.34
Damping ratio, ζ_w	0.032
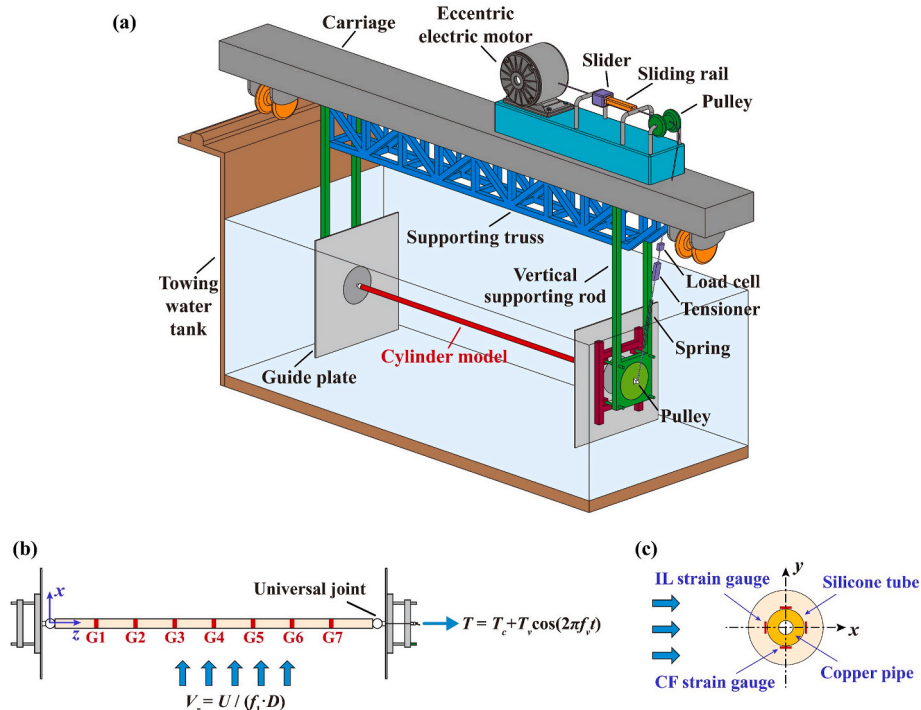
Fig. 1. Schematic diagram of the experimental apparatus: (a) Axonometric view, (b) Loading scheme and strain gauges arrangement, and (c) Cross-sectional view.

Table 2
Test matrix.

Excitation parameters		Values	
Time-varying axial-tension excitation	Amplitude ratio, T_v/T_c	0.1, 0.2, 0.3	
	Amplitude, T_v (N)	40, 80, 120	
	Frequency ratio, f_v/f_1	0.5, 1.0, 1.5, 2.0, 3.0	4.0
	Frequency, f_v (Hz)	1.17, 2.34, 3.69, 4.68, 7.38	9.36
VIV excitation	Towing velocity, U (m/s)	0.05: 0.05: 1.00	0.10: 0.10: 1.00
	Reduced velocity, V_r	1.34–26.71	2.67–26.71

cases was approximately 15 min.

2.2. Data process methodology

The bending strains of seven measurement points G1-G7 were obtained during the experiment. The bandpass filter process with a bandwidth of 1.0 Hz–40.0 Hz was first conducted on the strain signals to eliminate the unfavorable low-frequency vibration and high-frequency noise (Xu et al., 2021b). Subsequently, the modal analysis method was used to reconstruct the displacement of the cylinder model (Ma et al., 2020; Xu et al., 2018). The vibration displacement function at a given time during the experiment, taking the displacement in the CF direction $y(x,t)$ as an example, can be expressed as:

$$y(z,t) = \sum_{n=1}^{\infty} w_n(t) \cdot \varphi_n(z) \tag{2}$$

where $w_n(t)$ is the modal weight function, $\varphi_n(z)$ is the mode shape function, and n denotes the modal number varying from 1 to 7.

The simply supported flexible cylinder can be approximately regarded as a Bernoulli-Euler beam (Xu et al., 2020a). Based on this postulation, the bending strain of the cylinder can be obtained by differentiating the displacement function:

$$\frac{\varepsilon(z,t)}{R} = \frac{d^2 y(z,t)}{dz^2} \tag{3}$$

where $\varepsilon(z,t)$ is the bending strain function of an arbitrary point on the cylinder, R refers to the radius of the cylinder, and z refers to the coordinate of the point. Therefore, the stress function can be derived as:

$$\sigma(z,t) = E \cdot \varepsilon(z,t) = -\frac{ED}{2} \cdot \left(\frac{n\pi}{L}\right)^2 \sum_{n=1}^{\infty} \omega_n(t) \cdot \sin\frac{n\pi z}{L} \tag{4}$$

where E is the elastic modulus of the cylinder model and D is the diameter of the cylinder.

The continuous stress-time history function should be discretized according to a certain rule for the succeeding fatigue damage calculation. Herein, the rainflow counting method was employed to count the stress ranges and the corresponding number of cycles of the seven measurement points along the cylinder. Rainflow counting method is widely applied in civil engineering and offshore engineering for load-time history counting and damage calculation. The rainflow counting method generally includes the following steps (Xu et al., 2020b):

- Simplify the strain-time history spectrum.
- Choose a starting peak (or valley) point, and the raindrop fall down the spectrum according to some rules.
- Extract the complete cycles, rearrange the residual spectrum, and repeat the process.
- Record the strain ranges, mean value, and number of cycles of all the complete cycles.

Detailed processes have been introduced in previous research (Lu et al., 2023).

After obtaining the discrete stress ranges and their frequencies, the fatigue damage of the cylinder is evaluated based on the *S–N* curve method stipulated in , which is presented as:

$$\log N_i = \log \overline{a} - m \cdot \log \Delta \sigma_i \tag{5}$$

where $\log\overline{a}$ and m are material parameters depending on the geometrical arrangement, fabrication method, and environment of the specimen. In this paper, given the experimental environment and material properties of the flexible cylinder, the B1 *S–N* curve for free corrosion in seawater is adopted, i.e., $\log\overline{a} = 12.436$ and $m = 3.0$.

The general *S–N* curve is for the constant-amplitude fatigue damage evaluation. Therefore, for a random load spectrum, the total fatigue damage is calculated as the summation of all fatigue damage. To simplify the calculation, it is assumed that the accumulative fatigue damage of the cylinder is independent of the loading sequence. Therefore, based on the Palmgren-Miner linear accumulative damage rule, the total fatigue damage of the cylinder is expressed by:

$$D_{\text{total}} = \sum_{i=1}^{}\frac{n_i}{N_i} \tag{6}$$

Substituting the results of the rainflow counting method into the simultaneous equations of Eq. (5) and Eq. (6), the accumulative fatigue damage at any point on the cylinder can be calculated as:

$$D_{total}(z/L) = \frac{1}{\overline{a}} \sum_{i=1}^{} n_i \cdot \Delta \sigma_i^m \tag{7}$$

where z denotes the coordinate of an arbitrary point and L denotes the length of the cylinder.

3. Results and discussions

3.1. Strain response

Fig. 2 presents an illustrative example of the spatiotemporal CF strain distribution of the flexible cylinder at $V_r = 10.68$. The CF vibration of the cylinder under pure VIV excitation exhibits a standing wave feature (as shown in Fig. 2(a)). After applying the axial tension excitation, the CF response of the cylinder alters from a standing wave to a traveling wave characteristic. This phenomenon is in accordance with some previous research that the heave-induced vertical motion of the cylinder exhibits a typical traveling wave feature (Wang et al., 2014). In addition, the vibration frequency of the cylinder under the combined excitation is significantly increased compared with that under pure VIV excitation in some cases (see Fig. 2(b) and (c)). Similarly, the IL response of the cylinder also demonstrates a combination of standing and traveling waves under the combined VIV and axial-tension excitations, but the vibration frequency increase is imperceptible.

Furthermore, when the root mean square (RMS) strain distribution of the flexible cylinder was analyzed, the influence of the time-varying axial-tension excitation on the cylinder vibration is apparent. The root mean square (RMS) strain is written as:

$$\varepsilon_{\text{RMS}}(z) = \sqrt{\frac{1}{s} \sum_{i=1}^{s} \varepsilon^2(z,t)} \tag{8}$$

where s is the number of time samples. Therefore, two examples of the RMS strain distribution of the cylinder under different excitation amplitudes and frequencies are illustrated in Figs. 3 and 4.

The axial tension amplitude has a pronounced influence on the RMS strain distribution of the cylinder. Fig. 3 presents the CF RMS strain curves of the cylinder under the axial tension excitation frequency ratio of $f_v/f_1 = 2.0$ (i.e., $f_v = 4.68$ Hz). The VIV of the cylinder cannot be excited at small reduced velocities (when $V_r \leq 4.01$), and the vibration
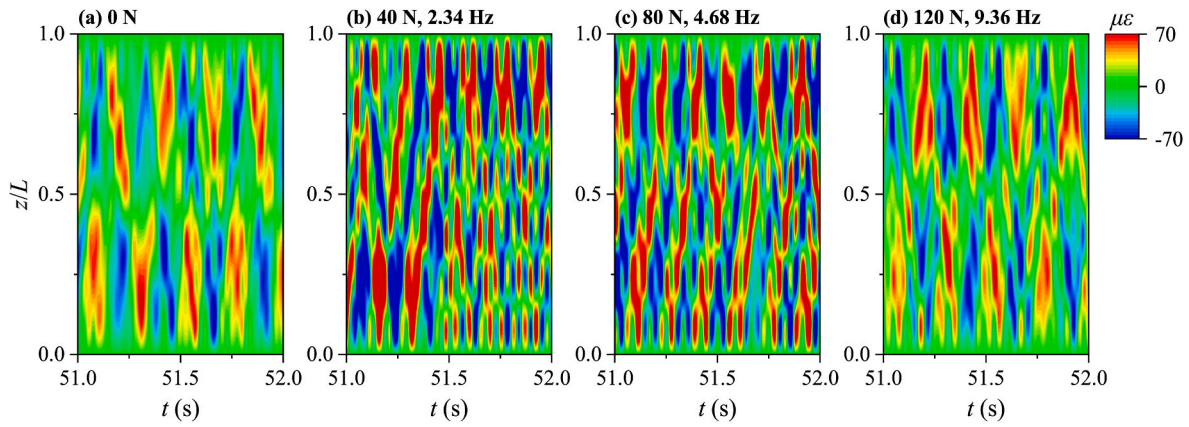
Fig. 2. Contours of the spatiotemporal CF strain variations of the flexible cylinder at $V_r = 10.68$: (a) $T_v = 0$ N, (b) $T_v = 40$N, $f_v = 2.34$ Hz, (c) $T_v = 80$N, $f_v = 4.68$ Hz, and (d) $T_v = 120$N, $f_v = 9.36$ Hz.
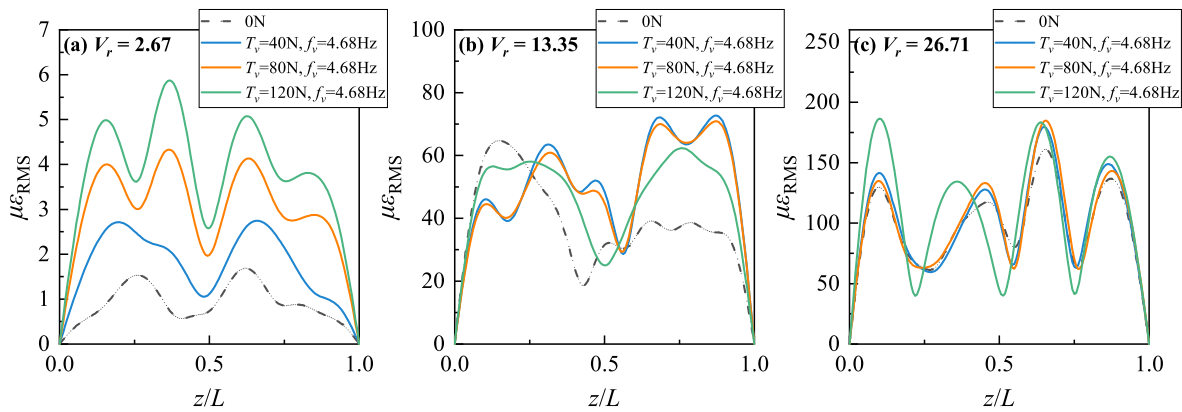
Fig. 3. Comparison of spanwise CF RMS strain distribution of the cylinder with $f_v/f_1 = 2.0$ and $T_v/T_c = 0.1$–0.3: (a) $V_r = 2.67$, (b) $V_r = 13.35$, and (c) $V_r = 26.71$.
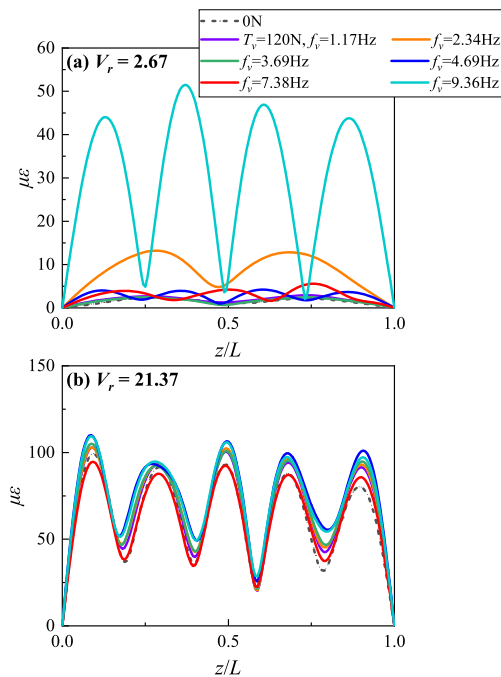
Fig. 4. Comparison of the spanwise IL RMS strain distribution of the flexible cylinder with $T_v = 120$ N ($T_v/T_c = 0.3$) and $f_v/f_1 = 0.5$–4.0: (a) $V_r = 2.67$ and (b) $V_r = 21.37$.

of the cylinder is mainly dominated by the time-varying axial tension excitation. For example, when $V_r = 2.67$ (see Fig. 3(a)), the cylinder vibrates slightly under pure VIV but the vibration is greatly enhanced after applying the axial tension excitation due to the parametric resonance. For the parametric excitation with $f_v/f_1 = 2.0$, the cylinder shows resonance behaviour of significant vibration enhancement and new local peak of RMS modal displacement, as the time-varying excitation may change the natural frequency of the cylinder. The CF vibration and CF RMS strain are increased with the increase of the axial tension amplitude ratio. Although only the 1st-order mode vibration is excited when $V_r = 2.67$, the maximum CF RMS strain of the cylinder is increased by 62.8%, 156.9%, and 248.3% under axial tension amplitude ratios of 0.1, 0.2, and 0.3, respectively, compared to that under pure VIV excitation. When $V_r \geq 4.01$, the VIV of the cylinder occurs. As the reduced velocity increases, the higher-order mode vibrations are excited. The axial tension has a less significant effect on the maximum RMS strain of the cylinder but affects the vibration mode and dominant frequency (Ma et al., 2020). The increase of excitation amplitude or frequency can excite the higher-order mode vibration of the cylinder at lower reduced velocities and widen the mode resonance regions. When $V_r = 13.35$, the 1st-order and 2nd-order mode vibrations are excited. Therefore, the RMS strain curves show four peaks under pure VIV excitation and five peaks under concomitant excitation (see Fig. 3(b)). Notably, the RMS strain distributions are approximately equal for the cases of $T_v = 40$ N and 80 N, but the maximum RMS strain decreases slightly when T_v increases to 120 N, which is also somewhat consistent with the tendency of the spatiotemporal strain distribution in Fig. 2. As the reduced velocity increases, the axial tension amplitude ratio has a relatively weak effect on the vibration of the cylinder. When $V_r = 26.71$, the 3rd- and 4th-order

mode vibration are excited, the RMS strain distribution curves of the cylinder with axial excitation amplitude ratio of 0.1 and 0.2 are approximately the same as the curve of the cylinder with $T_v = 0$ N. In addition, the axial tension excitation increases the maximum RMS strain of the cylinder by less than 15%, compared with the pure VIV excitation.

On the other hand, the axial tension frequency ratio also greatly affects the RMS strain of the cylinder. Fig. 4 exemplifies an example of the IL RMS strain curves of the cylinder considering different excitation frequencies. When $V_r = 2.67$ (see Fig. 4(a)), the IL VIV is also not excited at low reduced velocities, and the RMS strains of the cylinder are enhanced under the excitation of axial tension, especially for $f_v/f_1 = 1.0$ and $f_v/f_1 = 4.0$. When $f_v/f_1 = 1.0$ (i.e., $f_v = 2.34$ Hz), the excitation frequency is close to the 1st-order natural frequency of the cylinder model. A significant 2nd-order mode vibration occurs on the cylinder. Therefore, the vibration is enhanced and RMS strain is increased greatly. For the case of $f_v = 9.36$ Hz, the time-varying excitation is located in the second-order instability region according to Floquet's theory and the 4th-order mode resonance is excited (Ma et al., 2020), so that the cylinder vibrates violently and the IL RMS strain is significantly increased by approximately 25 times compared with that under pure VIV. As the reduced velocity is increased, the higher-order mode vibrations of the cylinder can be excited. The application of axial tension excitation can allow the IL vibration of the cylinder to enter higher-order vibration at lower reduced velocities compared with the pure VIV. However, the effect of the axial tension frequency ratio on RMS strain is relatively imperceptible when the VIV is greatly excited. When $V_r = 21.37$, the 5th-order mode vibration is excited and the spanwise RMS strain distributions of the cylinder present five peaks regardless of the excitation frequency, as shown in Fig. 4(b), but the maximum RMS strain is increased by approximately 10.8% at most. The RMS strain distribution and the maximum RMS strain are not significantly related to the excitation frequency.

3.2. Fatigue damage distribution

The response characteristics indicate that the time-varying axial tension has a considerable effect on the cylinder. Therefore, it is asserted that this axial excitation can also alter the fatigue damage characteristics of the cylinder to some extent. The fatigue damage distribution characteristics of the cylinder are examined in this section with regard to different excitation amplitudes and excitation frequencies.

Figs. 5 and 6 depict the accumulative fatigue damage distribution contours of the cylinder under $T_v/T_c = 0.1$ ($T_v = 40$ N) and $f_v/f_1 = 0.5$–4.0 in the IL and CF directions, respectively. Clearly, as the reduced velocities increases, the IL vibration of the cylinder is enhanced and the fatigue damage is aggravated. Higher-order mode vibrations contribute considerably to the vibration and multimode vibration occurs. However, it seems that the time-varying excitation negligibly influences the fatigue damage distribution under a relatively small axial tension amplitude ratio ($T_v/T_c = 0.1$). In the IL direction (see Fig. 5), the fatigue damage of the cylinder increases slightly with the increase of the axial tension excitation frequency ratio, but the effect of frequency ratio on the fatigue damage distribution is not conspicuous, except for the case of $f_v/f_1 = 4.0$. The fatigue damage of the cylinder is mainly affected by the reduced velocity of the VIV excitation. For the cases of $f_v/f_1 = 1.0$–3.0 (see Fig. 5(a)–5(e)), the accumulative fatigue damage distributions share an analogous tendency. When $V_r \leq 5.34$, the fatigue damage is relatively moderate and is uniformly distributed along the cylinder since the VIV has not been excited. The axial tension excitation leads to the 1st- and 2nd-order moder vibration of the cylinder, especially for the case of $f_v/f_1 = 1.0$ (Ma et al., 2020). When $5.34 \leq V_r \leq 10.68$, approximately 4 serious fatigue damage regions appear on the cylinder. As the reduced velocity increases, high-order mode IL vibrations are excited and the fatigue damage of the cylinder is intensified. The 3rd- and 4th-order mode IL vibrations are excited when $V_r \geq 9.34$ and $V_r \geq 14.69$. When $V_r \geq 18.70$, the severe fatigue damage region increases from 4 to 5 and the cylinder suffers from more serious maximum fatigue damage. In addition, for the case of $f_v = 9.36$ Hz (see Fig. 5(f)), when the reduced velocity is small to excite the VIV of the cylinder (i.e., $V_r \leq 5.34$), the fatigue damage of the cylinder is moderately aggravated compared with that of the cylinder under other excitation frequencies. In these cases, the cylinder vibrates mildly in the vortex street; thus, the fatigue damage
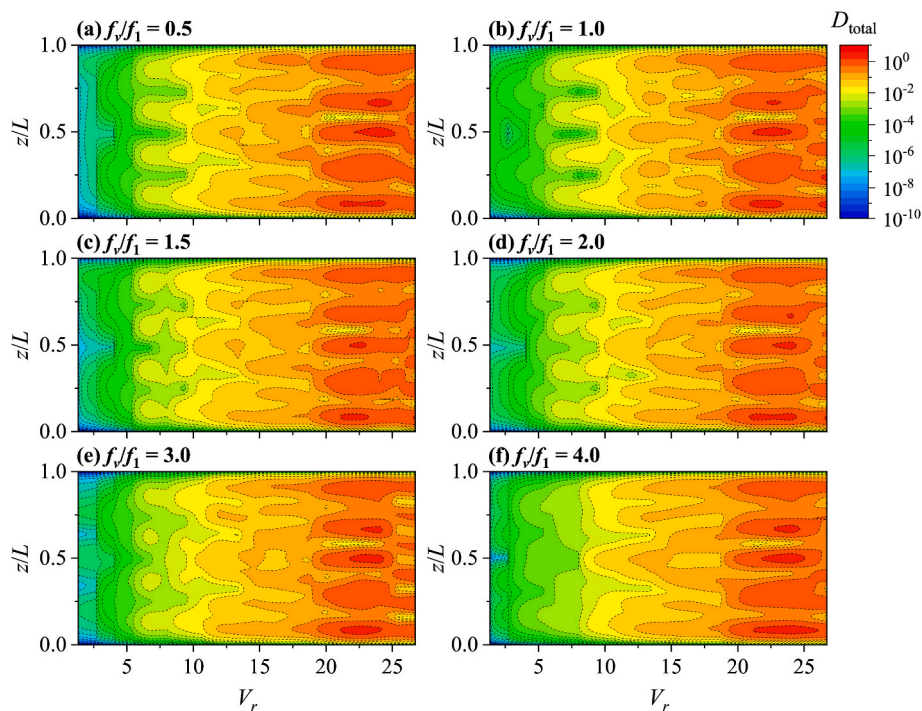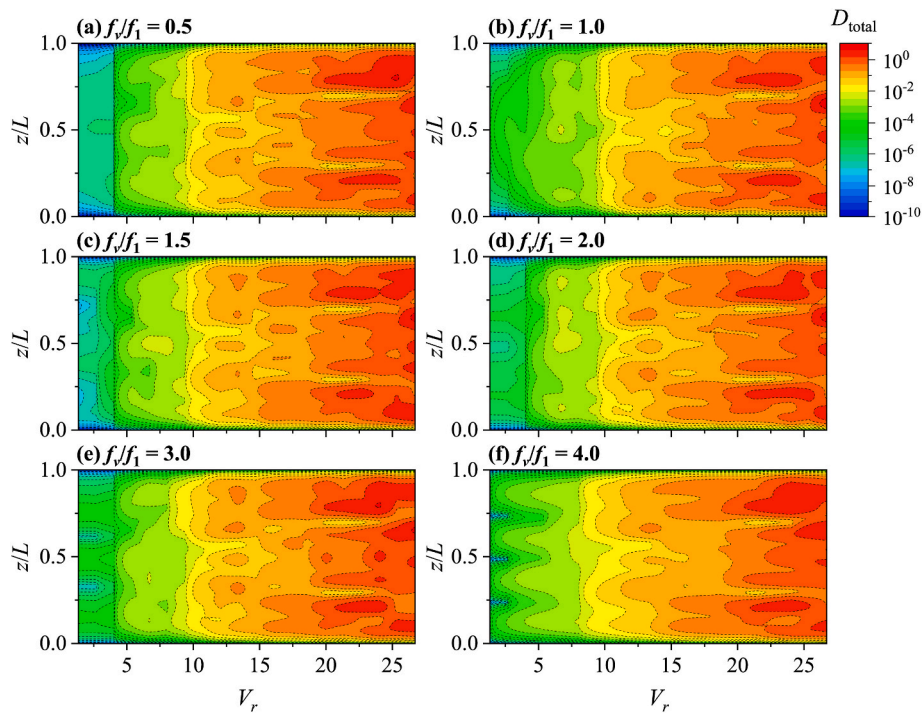

Fig. 5. Accumulative IL fatigue damage distribution contours of the cylinder with $T_v/T_c = 0.1$ ($T_v = 40$ N): (a) $f_v/f_1 = 0.5$, (b) $f_v/f_1 = 1.0$, (c) $f_v/f_1 = 1.5$, (d) $f_v/f_1 = 2.0$, (e) $f_v/f_1 = 3.0$, and (f) $f_v/f_1 = 4.0$.

Fig. 6. Accumulative CF fatigue damage distribution contours of the cylinder for $T_v/T_c = 0.1$ ($T_v = 40$ N): (a) $f_v/f_1 = 0.5$, (b) $f_v/f_1 = 1.0$, (c) $f_v/f_1 = 1.5$, (d) $f_v/f_1 = 2.0$, (e) $f_v/f_1 = 3.0$, and (f) $f_v/f_1 = 4.0$.

is primarily caused by high-frequency axial tension excitation. When $8.01 \leq V_r \leq 18.70$, three severe fatigue damage regions occur on the cylinder and the mid-span region of the cylinder withstands the most severe fatigue damage. When $V_r \geq 18.70$, the fatigue damage distribution exhibits the same characteristics as that under other frequency ratios that approximately five serious fatigue damage regions distribute evenly along the cylinder.

On the other hand, different from that in the IL direction, the CF fatigue damage distribution demonstrates distinct characteristics depending on the excitation frequency. When the excitation frequency approximates the natural frequency of the cylinder (i.e., $f_v = f_1$), an obvious fatigue damage aggravation is observed along the cylinder when $V_r \leq 5.34$ (see Fig. 6 (b)). The VIV is not excited at small reduced velocities, and the vibration is mainly induced by axial tension excitation. The cylinder vibrates violently because the 1st-order mode vibration is considerably excited, especially for the case of $f_v/f_1 = 1.0$. Similar fatigue damage aggravations are also observed when $f_v = 2.0 \cdot f_1$ and $f_v = 3.0 \cdot f_1$ due to the occurrence of the multimode vibrations (Franzini et al., 2018; Ma et al., 2020). However, the fatigue damage is dominated by the VIV at larger reduced velocities ($V_r \geq 10.68$). The fatigue damage becomes more serious with the increase of the reduced velocity. The severe damage regions extend due to the mode resonance caused by VIV. However, the fatigue distribution characteristics show no significant differences when applying the tension excitation with varying frequency ratios. As the results show, the cylinder approximately sustains the same spanwise fatigue damage distribution for the case of $f_v/f_1 = 0.5$–3.0. It is inferred that the effect of the tension frequency on the fatigue damage is non-significant due to the small tension amplitude ratio. Similar to the case in the IL direction, the CF fatigue damage distribution under the excitation frequency $f_v = 9.36$ Hz shows more distinct characteristics (see Fig. 6(f)). The fatigue damage along the whole cylinder is greatly enhanced when $V_r \leq 16.03$. The motion trajectory analysis shows that the vibration trajectory width of the cylinder is considerably widened by the axial tension excitation with $f_v = 9.36$ Hz (Ma et al., 2020). Consequencly, the wide and disordered motion trajectories possibly mean a considerable energy transfer between the fluid and the cylinder model

under this excitation frequency, leading to severe fatigue damage.

As the excitation amplitude increases, the axial tension excitation has an increasingly significant effect on the fatigue damage distribution characteristics. The accumulative fatigue damage distribution contours of the cylinder under $T_v/T_c = 0.2$ ($T_v = 80$ N) and $f_v/f_1 = 0.5$–4.0 in the IL and CF directions are illustrated in Figs. 7 and 8, respectively.

The fatigue damage distribution of the cylinder under $T_v/T_c = 0.2$ shows relatively obvious variation with the increase of the tension frequency ratio, compared with that under $T_v/T_c = 0.1$. The tension excitation is more effective for the fatigue damage of the cylinder at large tension amplitudes. As the excitation frequency ratio is increased, the fatigue damage of the cylinder is progressively increased, which means that the cylinder's vibration is dominated by the axial tension excitation. Moreover, the fatigue damage aggravation is more distinct in the CF direction than in the IL direction. When $V_r \leq 5.34$, the fatigue damage distributes almost uniformly along the cylinder. However, four symmetrical peak fatigue damage regions appear earlier on the cylinder for $f_v = 9.36$ Hz in the IL direction (see Fig. 7(f)) and in the CF direction (see Fig. 8(f)). The fatigue damage is enhanced because the time-varying excitation allows the cylinder enter the higher-order vibration mode earlier and extends the resonance regions (Xu et al., 2020c). Moreover, the fatigue damage distribution of the cylinder subjected to the concomitant excitation demonstrates approximately similar patterns to the cylinder only subjected to pure VIV at high reduced velocities, indicating that the cylinder vibrates violently due to the vortex shedding instead of axial excitation. When $5.34 \leq V_r \leq 17.36$, the fatigue damage distribution of the cylinder tends to show similar characteristics to that without axial tension excitation, except for the case of $f_v = 9.36$ Hz. An aggravated fatigue damage region appears at the mid-span of the cylinder in the IL direction (see Fig. 7(f)). The width of the serious CF fatigue damage region is larger for $f_v/f_1 = 4.0$ than for other cases (see Fig. 8(f)). These differences also attest that the instability of the cylinder caused by the axial-tension excitation is a major concern for fatigue damage (Wang et al., 2015; Yang and Xiao, 2014). However, when $V_r \geq 20.03$, the fatigue damage is similarly distributed along the cylinder regardless of the excitation frequency and the values of the fatigue
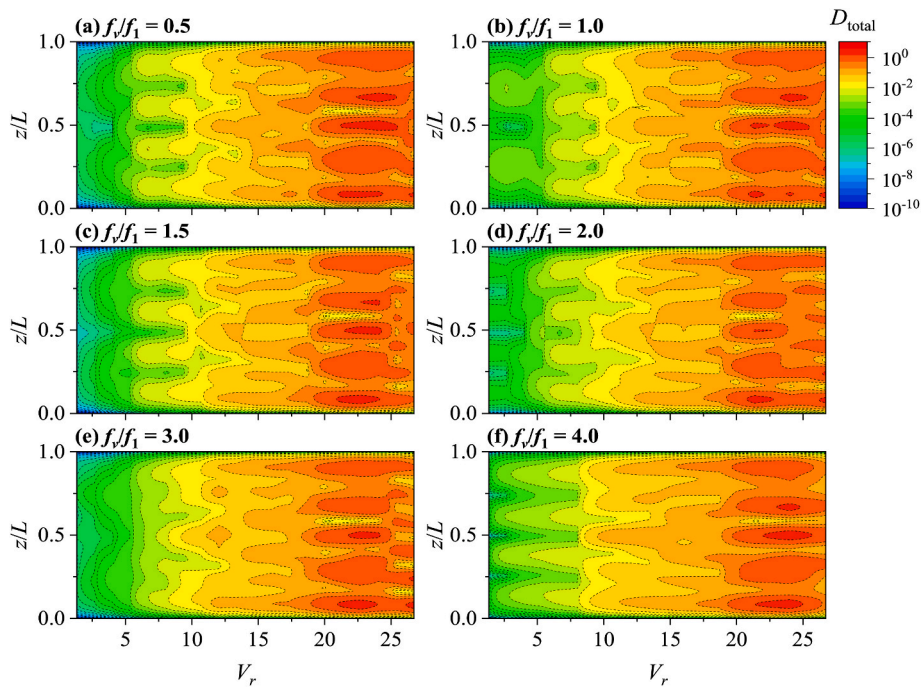
Fig. 7. Accumulative IL fatigue damage distribution contours of the cylinder with $T_v/T_c = 0.2$ ($T_v = 80$ N): (a) $f_v/f_1 = 0.5$, (b) $f_v/f_1 = 1.0$, (c) $f_v/f_1 = 1.5$, (d) $f_v/f_1 = 2.0$, (e) $f_v/f_1 = 3.0$, and (f) $f_v/f_1 = 4.0$.
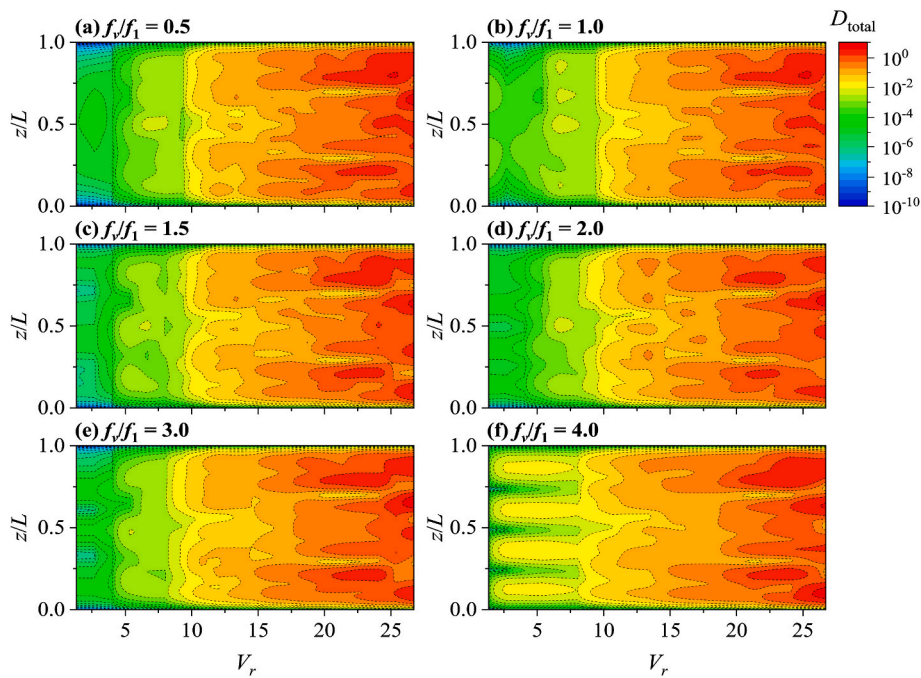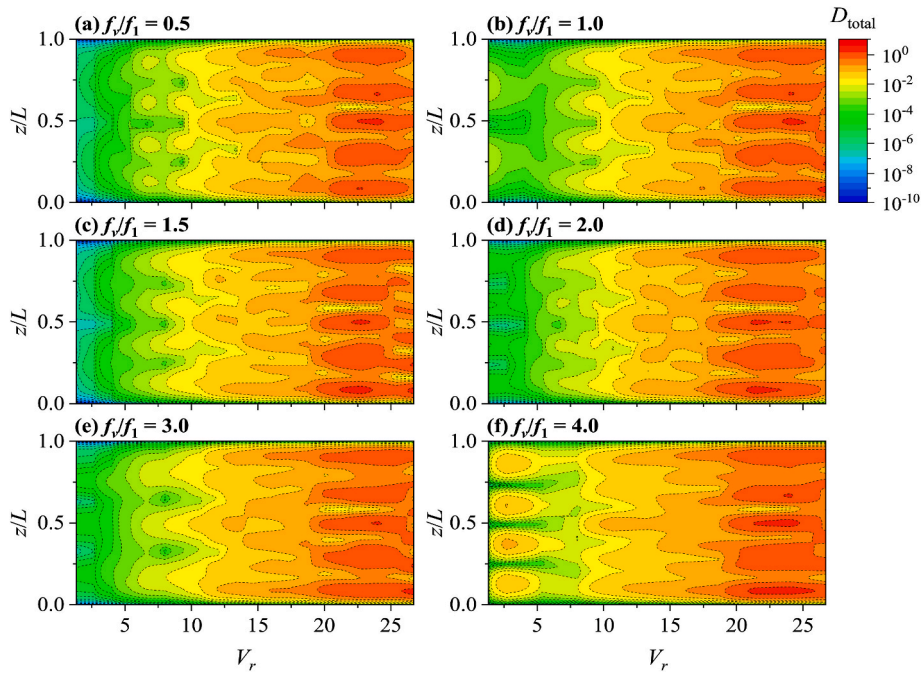

Fig. 8. Accumulative CF fatigue damage distribution contours of the cylinder with $T_v/T_c = 0.2$ ($T_v = 80$ N): (a) $f_v/f_1 = 0.5$, (b) $f_v/f_1 = 1.0$, (c) $f_v/f_1 = 1.5$, (d) $f_v/f_1 = 2.0$, (e) $f_v/f_1 = 3.0$, and (f) $f_v/f_1 = 4.0$.

damage show no significant difference, suggesting that VIV contributes prominently to the fatigue damage.

As the excitation amplitude ratio increases to 0.3 ($T_v = 120$ N), the large axial-tension amplitude significantly affects the fatigue characteristics of the cylinder. The influences of the excitation frequency f_v on the fatigue damage distribution under vortex-shedding and axial-tension excitation become more apparent. The IL and CF fatigue damage distribution contours for $T_v/T_c = 0.3$ ($T_v = 120$ N) and $f_v/f_1 = 0.5$–4.0 are shown in Figs. 9 and 10, respectively.

Similar to that under $T_v = 20$ N and $T_v = 40$ N, the fatigue damage distribution under $T_v = 120$ N also follows a tendency that the fatigue damage is enhanced at low reduced velocities due to the dominance of the axial tension excitation. However, it is noteworthy that the apparent variation of the fatigue damage distribution is observed for all excitation frequencies when $V_r \leq 5.34$ and the variation is the most pronounced for $f_v = 9.36$ Hz. The fatigue damage is greatly enhanced in both the IL and CF direction since higher-order mode resonances occurs with the increase of the frequency ratio. The fatigue damage for $f_v = 9.36$ Hz is

Fig. 9. Accumulative IL fatigue damage distribution contours of the cylinder with $T_v/T_c = 0.3$ ($T_v = 120$ N): (a) $f_v/f_1 = 0.5$, (b) $f_v/f_1 = 1.0$, (c) $f_v/f_1 = 1.5$, (d) $f_v/f_1 = 2.0$, (e) $f_v/f_1 = 3.0$, and (f) $f_v/f_1 = 4.0$.
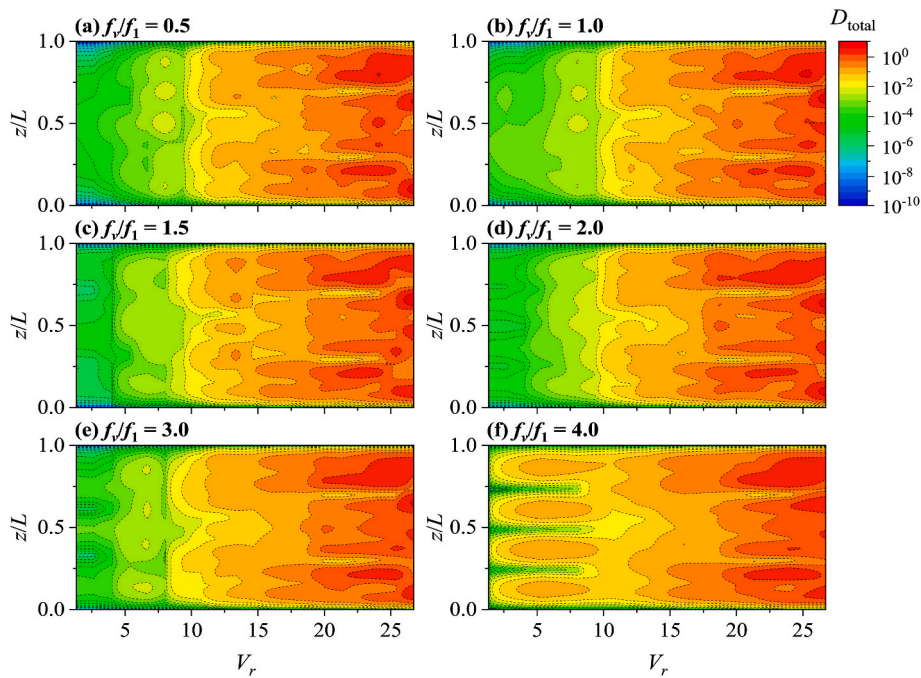
Fig. 10. Accumulative CF fatigue damage distribution contours of the cylinder with $T_v/T_c = 0.3$ ($T_v = 120$ N): (a) $f_v/f_1 = 0.5$, (b) $f_v/f_1 = 1.0$, (c) $f_v/f_1 = 1.5$, (d) $f_v/f_1 = 2.0$, (e) $f_v/f_1 = 3.0$, and (f) $f_v/f_1 = 4.0$.

enhanced when $V_r \le 5.34$ but is slightly suppressed when $5.34 \le V_r \le 10.68$ in the IL direction, as shown in Fig. 9(f). This variation indicates that, at high reduced velocities, the VIV is the main reason causing the mode vibration and fatigue damage while axial tension excitation slightly affects the fatigue damage. According to Ma et al., 2020, the 4th-order mode vibration of the cylinder is observed when $V_r = 2.67$ but the VIV only leads to the 2nd-order mode vibration when $V_r = 5.34$. An analogous distribution is also observed in the CF direction, as shown in Fig. 10(f). Four peak fatigue damage regions symmetrically appear on

the cylinder when $V_r \le 5.34$, but the fatigue damage is slightly suppressed when $5.34 \le V_r \le 10.68$. The value of the fatigue damage is larger in the CF direction than in the IL direction. The fatigue damage distribution difference between IL and CF directions can be explicated that the vortex shedding substantially affects the hydrodynamic lift coefficient and strengthens the instability of the cylinder, resulting in the enhancement of fatigue damage in the CF direction (Wu et al., 2021; Yang and Xiao, 2014). Moreover, as the reduced velocity continues to increase to 16.03, the cylinder exhibits approximately the same fatigue

damage distribution regardless of excitation frequency due to the predominance of VIV excitation. Although the tension excitation can slightly enlarge the resonance region and promote the mode vibration, its effect on the fatigue damage distribution is not significant when the reduced velocity is large.

3.3. Relative fatigue damage distribution

To further analyze the influence of the axial-tension excitation on the fatigue performance of the flexible cylinder, the accumulative fatigue damage distribution of the cylinder subjected to concomitant excitation was compared with that only subjected to VIV excitation (i.e., $T_v/T_c = 0$). The relative fatigue damage ratio was defined as follows:

$$D_R = \frac{D_{VIV-T} - D_{VIV}}{D_{VIV}} \quad (9)$$

where D_R is the relative fatigue damage ratio, D_{VIV-T} is the accumulative fatigue damage of the cylinder subjected to the simultaneous excitation of VIV and time-varying axial tension, and D_{VIV} is the accumulative fatigue damage of the cylinder only subjected to VIV excitation.

The relative accumulative IL fatigue damage ratio contours in the case of $T_v/T_c = 0.1$–0.3 and $f_v/f_1 = 1.0$, 2.0, and 4.0 are shown in Fig. 11. When $V_r \leq 5.34$, the cylinder sustains increasingly severe fatigue damage after applying the axial tension excitation. When the VIV is not excited, the time-varying excitation can excite the resonance of the

cylinder and primarily effects the fatigue damage. Seemingly, the IL fatigue damage is considerably aggravated with the increase of the excitation amplitude and the increase of the excitation frequency. For $f_v = f_1$, the fatigue damage aggravation region is slightly extended as the tension frequency ratio increases from 0.1 to 0.3 (see Fig. 11(a)). While for $f_v/f_1 \geq 1.5$, the fatigue damage is considerably enhanced and the fatigue enhancement region is enlarged with the increase of excitation frequency (see Fig. 11(b) and (c)). The effect of the excitation frequency on the fatigue damage enhancement region is more obvious for the case of $f_v/f_1 = 4.0$ (see Fig. 11(c)). Additionally, when $V_r \geq 5.34$, the VIV dominates the fatigue damage characteristics of the cylinder. The fatigue damage of the cylinder is considerably intensified at the quarter-span and mid-span positions, only when the reduced velocity is close to 10.68, 13.35, and 20.03. At other reduced velocities, the accumulative fatigue damage along the cylinder under the combined excitation is only slightly increased or even moderated than that under pure VIV excitation. This distribution characteristic is possibly due to the amplitude modulation of the VIV response caused by the axial tension excitation (Ma et al., 2020), which may limit the vibration and fatigue damage accumulation of the cylinder. Moreover, the amplitude modulation phenomenon becomes increasingly pronounced as the frequency increases, thereby slightly reducing the fatigue damage, as shown in the first column in Fig. 11. However, the fatigue damage is only decrease in some areas of the cylinder but the maximum fatigue damage of the cylinder is less affected.
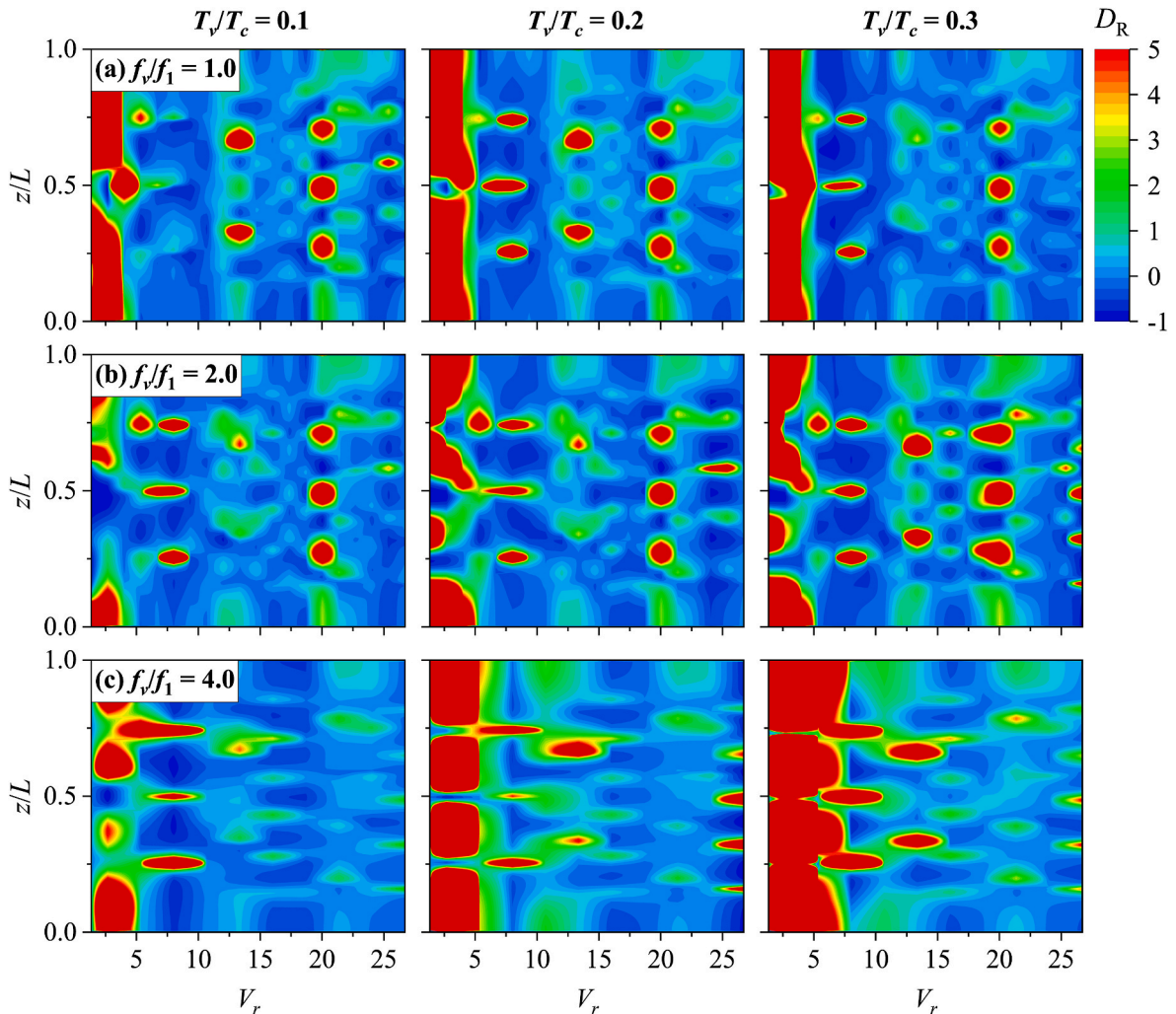

Fig. 11. Relative fatigue damage ratio distribution contours of the flexible cylinder in the IL direction for $T_v/T_c = 0.1$ (first column), $T_v/T_c = 0.2$ (second column), and $T_v/T_c = 0.3$ (third column): (a) $f_v/f_1 = 0.5$, (b) $f_v/f_1 = 1.0$, (c) $f_v/f_1 = 2.0$, and (c) $f_v/f_1 = 4.0$.

On the other hand, the tension amplitude also affects the relative accumulative fatigue damage of the cylinder. Fig. 12 presents the results in the CF direction under the axial tension excitation frequency ratio of $f_v/f_1 = 0.5$ (i.e., $f_v = 1.17$ Hz) is presented in. When the axial tension excitation frequency is relatively low, small tension amplitudes cannot excite obvious CF vibration of the cylinder at small reduced velocities. The spanwise fatigue damage is smaller than that under pure VIV excitation when $V_r \leq 5.34$ (see Fig. 12 (a) and (b)). When the excitation amplitude is increased to 80 N and 120N ($T_v/T_c = 0.2$ and 0.3), the effect of axial tension excitation becomes more obvious at small reduced velocities. The increasing tension amplitude leads to higher-order and more pronounced mode vibration, causing more severe CF fatigue damage to the cylinder. As the reduced velocity is increased, the CF fatigue damage is mainly caused by the VIV and the time-varying excitation does not significantly enhance the fatigue damage of the cylinder. Similarly, the CF fatigue damage in some regions along the cylinder is also suppressed at large reduced velocities, but the suppression effect becomes less remarkable with the increase in tension amplitude.

As the excitation frequency increases, the excitation amplitude manifests a pronounced effect on fatigue damage accumulation. For example, Fig. 13 illustrates the relative CF fatigue damage ratio contours for the case of $f_v/f_1 = 1.0$ ($f_v = 2.34$ Hz). At small reduced velocities when the VIV is not activated ($V_r \leq 5.34$), the fatigue damage is intensified for $T_v \leq 40$ N, which is quite different from the case of $f_v = 1.17$ Hz. Furthermore, the greater the excitation amplitude applied to the cylinder, the greater the fatigue damage that the cylinder would withstand. The enhanced fatigue damage region is extended and the relative fatigue damage ratio is increases as the excitation amplitude increases from 20 N ($T_v/T_c = 0.05$) to 120 N ($T_v/T_c = 0.3$) when the time-varying excitation dominates the cylinder vibration. When $5.34 \leq V_r \leq 10.68$, the spanwise fatigue damage of the cylinder is slightly more serious under the concomitant excitation than that under pure VIV excitation. Nevertheless, when $V_r \geq 10.68$, the axial tension excitation has nonsignificant influence on the fatigue damage aggravation.

In brief, both the axial-tension excitation amplitude and frequency have a considerable fatigue damage intensification effect on the cylinder when the VIV is not excited (i.e., $V_r \leq 5.34$). The larger the excitation amplitude and frequency are, the more serious the fatigue damage the cylinder would suffer from. This is because the axial tension can excite

more pronounced modal vibration of the cylinder. However, as the reduced velocity is increased to $V_r \geq 5.34$, VIV is excited and contributes considerably to the cylinder vibration and fatigue damage. The time-varying axial-tension excitation in such cases can somewhat alleviate the spanwise fatigue damage accumulation of the cylinder due to the amplitude modulation but it has little impact on the maximum fatigue damage of the cylinder.

3.4. Maximum fatigue damage

The variations of the maximum fatigue damage are also examined to investigate the influence of the excitation on the fatigue characteristics. The maximum fatigue damage is calculated as:

$$D_{\max} = \max_{0 \leq z/L \leq 1} \{D_{\text{total}}(z/L)\} \tag{10}$$

The maximum fatigue damage results of the cylinder for the axial tension amplitude ratio $T_v/T_c = 0.1$ ($T_v = 40$ N) and frequency ratio $f_v/f_1 = 0.1$–4.0 are depicted in Fig. 14. The fatigue damage caused by the time-varying excitation is obvious at low reduced velocities when $V_r \leq 4.01$. The axial tension excitation causes more serious fatigue damage in the IL direction than in the CF direction. The maximum fatigue damage is enhanced in both the IL and CF directions for $f_v = 2.34$ Hz ($f_v/f_1 = 1.0$) due to the 1st-order mode vibration and for $f_v = 9.36$ Hz ($f_v/f_1 = 4.0$) due to the instability resonance. But the maximum fatigue damage is slightly reduced for other excitation frequencies. For example, at $V_r = 2.67$, the maximum IL fatigue damage is increased by approximately 10 times for $f_v = 2.34$ Hz (i.e., $f_v/f_1 = 1.0 \cdot f_1$) but decreased by approximately 50% for the case of $f_v = 7.38$ Hz ($f_v/f_1 = 3.0$). The small tension frequency ratio can somewhat suppress the maximum IL and CF fatigue damage of the cylinder at small reduced velocities. Furthermore, as the reduced velocity is increased to 5.34, the VIV contributes more to the IL and CF maximum fatigue damage, while the excitation frequency has an imperceptible effect on the maximum fatigue damage. With the increase in the reduced velocity V_r, maximum fatigue damage value increases monotonically in both the IL and CF directions, since the high-order mode vibration can be gradually excited. However, the value is almost regardless of the excitation frequency.

For the $T_v = 80$ N case, the tension amplitude ratio approaches 0.2. The time-varying excitation effect is enhanced. The maximum fatigue
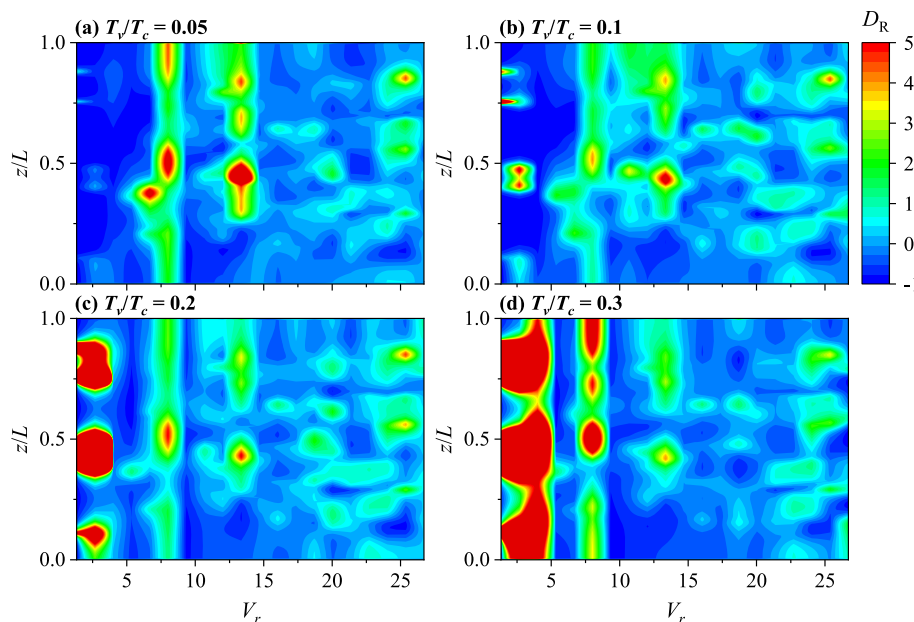

Fig. 12. Relative fatigue damage ratio distribution contours in the CF direction for $f_v/f_1 = 0.5$ ($f_v = 1.17$ Hz): (a) $T_v/T_c = 0.05$, (b) $T_v/T_c = 0.1$, (c) $T_v/T_c = 0.2$, and (d) $T_v/T_c = 0.3$.
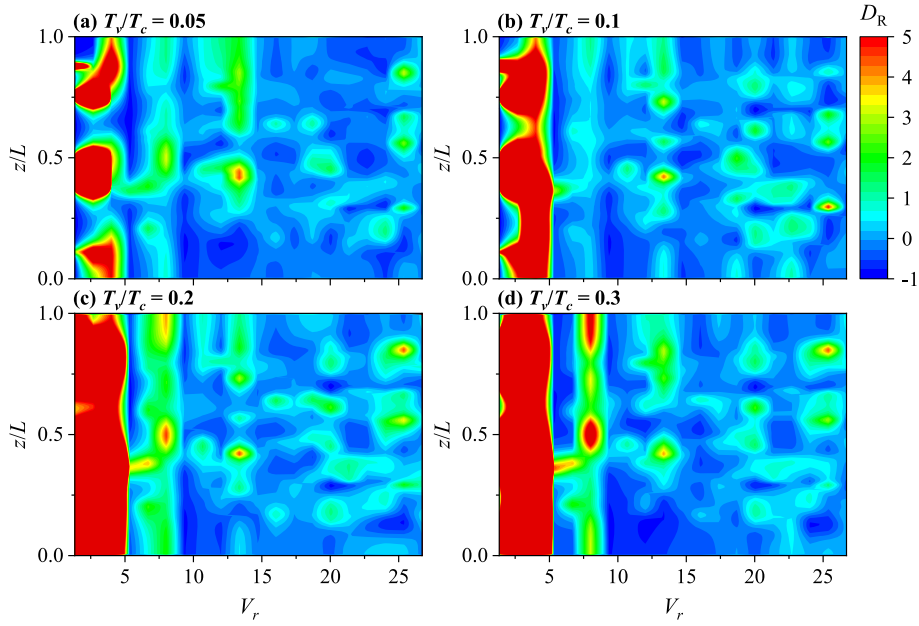
Fig. 13. Relative fatigue damage ratio distribution contours in the CF direction for $f_v/f_1 = 1.0$ ($f_v = 2.34$ Hz): (a) $T_v/T_c = 0.05$, (b) $T_v/T_c = 0.1$, (c) $T_v/T_c = 0.2$, and (d) $T_v/T_c = 0.3$.
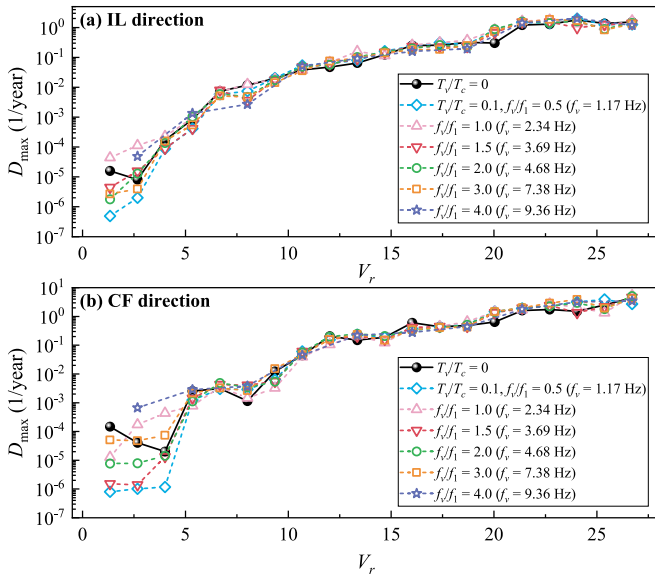

Fig. 14. Maximum fatigue damage of the cylinder versus reduced velocity for $T_v/T_c = 0.1$ ($T_v = 40$ N), with $f_v/f_1 = 0.5$–4.0 ($f_v = 1.17$–9.36 Hz): (a) IL direction and (b) CF direction.
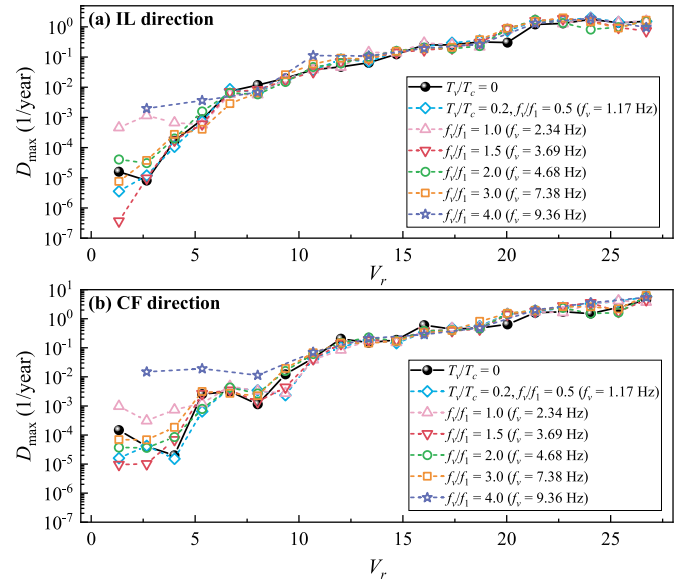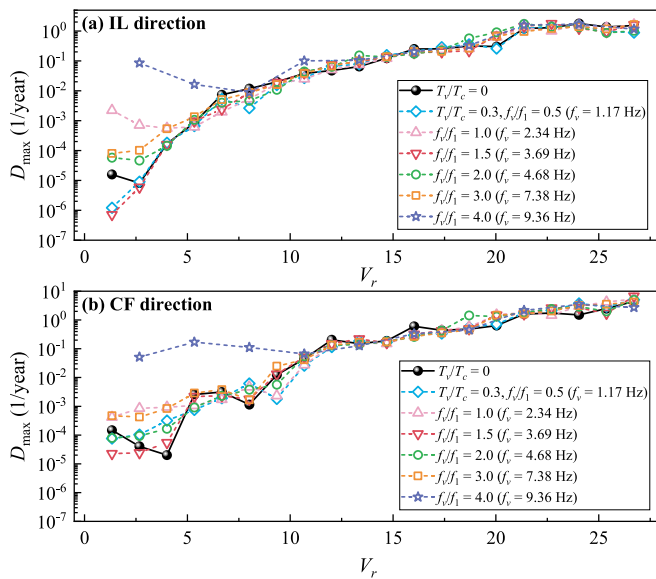
Fig. 15. Maximum fatigue damage of the cylinder versus reduced velocity for $T_v/T_c = 0.2$ ($T_v = 80$ N), with $f_v/f_1 = 0.5$–4.0 ($f_v = 1.17$–9.36 Hz): (a) IL direction and (b) CF direction.

damage for the case of $T_v/T_c = 0.2(T_v = 80$ N) and $f_v/f_1 = 0.1$–4.0 are shown in Fig. 15. At low reduced velocities (when $V_r \leq 4.01$), the cylinder suffers from larger maximum fatigue damage under the excitation amplitude of $f_v = 80$ N, compared with that under the excitation amplitude of $T_v = 40$ N. In addition, the axial tension excitation with $f_v = 9.36$ Hz (i.e., $f_v = 3.0 \cdot f_1$) causes considerable fatigue damage to the cylinder, especially in the CF direction. According to the previous analysis, the case of $T_v = 80$ N and $f_v = 9.36$ Hz is located in the second-order instability region (Ma et al., 2020). Therefore, the sharp increase in the maximum fatigue damage indicates that the instability of the cylinder can result in the significant mode resonance and severe fatigue damage of the cylinder. Similar to the case of $T_v = 40$ N, the maximum fatigue damage is highly affected by the VIV when $V_r \geq 9.34$. The maximum fatigue damage is greatly increased by increasing the reduced

velocity increases, but is slightly increased by applying different tension frequency ratios.

For the $T_v = 120$ N case, the tension amplitude ratio increases to 0.3. This increase in T_v has a considerable effect on the maximum fatigue damage of the cylinder. Fig. 16 presents the maximum fatigue damage results of the cylinder under the axial tension excitation with $T_v = 120$ N ($T_v/T_c = 0.2$) and $f_v/f_1 = 0.1$–4.0. Obviously, the tension excitation increasingly contributes to the fatigue damage characteristics of the cylinder under a large tension amplitude ratio of $T_v/T_c = 0.3$. Before the VIV is excited, the axial tension excites the violent vibration of the cylinder, leading to significant maximum fatigue damage. The maximum fatigue damage of the cylinder under the combined excitation is significantly larger than that under pure VIV excitation in IL and CF directions, except for a few cases. In the cases of $f_v = 2.34$ Hz, 7.38 Hz,

Fig. 16. Maximum fatigue damage of the cylinder versus reduced velocity for $T_v/T_c = 0.3$ ($T_v = 120$ N), with $f_v/f_1 = 0.5$–4.0 ($f_v = 1.17$–9.36 Hz): (a) IL direction and (b) CF direction.

and 9.36 Hz ($f_v/f_1 = 1.0$, 2.0, and 4.0), the maximum fatigue damage is enlarged greatly due to the multimode resonance. After the vortex shedding occurs, although the VIV mainly contributes to the fatigue damage, the maximum fatigue damage is still slightly increased under the excitation of axial tension. This slight fatigue damage intensification tendency is more distinct than that for the cases of $T_v = 40$ N and $T_v = 80$ N.

4. Conclusions

Model tests are performed to study the fatigue damage characteristics of a flexible cylinder under the concomitant excitation of vortex-induced vibration (VIV) and time-varying axial tension. Twenty reduced velocities (i.e., $V_r = 1.34$–26.71), three axial-tension amplitude ratios (i.e., $T_v/T_c = 0.1$, 0.2, and 0.3.) and six axial-tension frequency ratios (i.e., $f_v/f_1 = 0.5$, 1.0, 1.5, 2.0, 3.0, and 4.0.) are tested in this experiment. Based on the S–N curve method and linear fatigue damage accumulation theory, the RMS strain distribution, fatigue damage distribution, and maximum fatigue damage are discussed. Some primary conclusions are drawn as follows.

(1) The time-varying excitation considerably affects the dynamic response of the cylinder. A typical traveling wave pattern and an increase in vibration frequency are observed when the time-varying axial tension excitation is applied. At low reduced velocities (i.e., $V_r \leq 5.34$), the RMS strain curve and maximum RMS strain are significantly enhanced with the increase of the axial tension amplitude ratio and axial tension frequency ratio because the higher-order mode vibration is excited. In contrast, as the reduced velocity increases ($V_r \geq 5.34$), the axial excitation slightly alters the RMS strain distribution but marginally affects the maximum RMS strain.

(2) The accumulative fatigue damage distribution of the cylinder under combined excitation shows significantly different characteristics from that under pure VIV. At low reduced velocities ($V_r \leq 4.01$), the axial excitation dominates the fatigue damage and the VIV is not excited. The spanwise fatigue damage of the cylinder can be exacerbated with the increase of the axial tension amplitude or axial tension frequency, since the mode vibration is excited by the tension excitation. For small axial tension

amplitude ($T_v/T_c = 0.1$), the tension excitation imperceptibly affects the fatigue distribution unless the frequency ratio is large. Nevertheless, at high reduced velocities ($V_r \geq 5.34$), the fatigue damage is mainly induced by the VIV excitation. The cylinder exhibits higher-order mode vibrations and sustains more severe fatigue damage as the reduced velocity increases. The reduced velocity mainly determines the fatigue damage distribution patterns while the axial tension excitation slightly changes the distribution and value of the fatigue damage. However, the axial tension excitation can somewhat mitigate the accumulative IL and CF fatigue damage in some regions along the cylinder at high reduced velocities due to the amplitude modulation phenomenon.

(3) The maximum fatigue damage is greatly affected by the axial tension excitation at small reduced velocities (when $V_r \leq 4.01$). When the axial tension amplitude is small ($T_v/T_c = 0.1$), the maximum CF fatigue damage is decreased greatly under the axial tension excitation, except for some cases of $f_v/f_1 = 1.0$ and 4.0. As the excitation amplitude ratio increases to 0.2 and 0.3, the maximum fatigue damage of the cylinder is considerably enhanced in the IL and CF direction due to the multimode vibration of the cylinder. For a large tension amplitude ratio ($T_v/T_c = 0.3$) or a frequency ratio ($f_v/f_1 = 4.0$), the axial tension excitation has a significant influence on the variation of the maximum fatigue damage even at $V_r = 8.01$. However, at high reduced velocities (when $V_r \geq 5.34$), the maximum fatigue damage is primarily influenced by the reduced velocity. The maximum IL and CF fatigue damage increases with the enhancement of VIV, but is not significantly affected by the variation of the axial tension excitation.

Hopefully, these findings can contribute to a comprehensive understanding of the fatigue damage characteristics of the cylinder under coupling excitations and provide a reference for the fatigue design and damage suppression of analogous marine cylindrical structures. Nevertheless, there are some limitations in the current research. The conclusions are only valid for tensioned cylinders with low damping ratios, because the model tests were conducted on a cylinder with $\zeta_w = 0.032$, which may be controlled by limit cycle behaviour. The results may differ for a cylinder with higher structural damping or in a sheared flow. Besides, only several specific cases were tested in this study and some important phenomena may have been neglected. Therefore, future study should focus on the cylinder with varying specifications and cover more scenarios of reduced velocity and axial-tension excitation. This will enable comprehensive understanding of the fatigue characteristics and mechanism of cylindrical structures under combined excitation.

CRediT authorship contribution statement

Yan Lu: Methodology, Supervision. **Zhenchao Yu:** Visualization, Writing – review & editing. **Yexuan Ma:** Conceptualization, Methodology, Investigation. **Zhanxiang Liu:** Investigation, Writing – original draft. **Wanhai Xu:** Conceptualization, Methodology, Writing – review & editing.

Declaration of competing interest

All authors of this manuscript have directly participated in the planning, execution, and/or analysis of this study. The contents of this manuscript have not been copyrighted or published previously. The contents of this manuscript are not now under consideration for publication elsewhere. There are no directly related manuscripts or abstracts, published or unpublished, by any authors of this manuscript.

Data availability

Data will be made available on request.

Acknowledgement

References

Chen, W., Li, M., Zheng, Z., Guo, S., Gan, K., 2015. Impacts of top-end vessel sway on vortex-induced vibration of the submarine riser for a floating platform in deep water. Ocean. Eng. 99, 1–8.

Drumond, G.P., Pasqualino, I.P., Pinheiro, B.C., Estefen, S.F., 2018. Pipelines, risers and umbilicals failures: a literature review. Ocean. Eng. 148, 412–425.

Fan, Y., Mao, H., Guo, H., Liu, Q., Li, X., 2015. Experimental investigation on vortex-induced vibration of steel catenary riser. China Ocean Eng. 29 (5), 691–704.

Franzini, G.R., Mazzilli, C.E.N., 2016. Non-linear reduced-order model for parametric excitation analysis of an immersed vertical slender rod. Int. J. Non Lin. Mech. 80, 29–39.

Franzini, G.R., Pesce, C.P., Salles, R., Gonçalves, R.T., Fujarra, A.L.C., Mendes, P., 2015. Experimental analysis of a vertical and flexible cylinder in water: response to top motion excitation and parametric resonance. J. Vib. Acoust. 137 (3), 031010.

Franzini, G.R., Santos, C.C.P., Mazzilli, C.E.N., Pesce, C.P., 2016. Parametric excitation of an immersed, vertical and slender beam using reduced-order models: influence of hydrodynamic coefficients. Marine Systems & Ocean Technology 11 (1–2), 10–18.

Franzini, G.R., Pesce, C.P., Gonçalves, R.T., Fujarra, A.L.C., Mendes, P., 2018. An experimental investigation on concomitant Vortex-Induced Vibration and axial top-motion excitation with a long flexible cylinder in vertical configuration. Ocean. Eng. 156, 596–612.

Ge, F., Long, X., Wang, L., Hong, Y., 2009. Flow-induced vibrations of long circular cylinders modeled by coupled nonlinear oscillators. Sci. China G 52 (7), 1086–1093.

Gu, J., Dai, B., Wang, Y., Li, M., Duan, M., 2016. Dynamic analysis of a fluid-conveying pipe under axial tension and thermal loads. Ships Offshore Struct. 12 (2), 262–275.

Han, Q., Ma, Y., Xu, W., Fan, D., Wang, E., 2018a. Hydrodynamic characteristics of an inclined slender flexible cylinder subjected to vortex-induced vibration. Int. J. Mech. Sci. 148, 352–365.

Han, Q., Ma, Y., Xu, W., Zhang, S., 2018b. An experimental study on the hydrodynamic features of two side-by-side flexible cylinders undergoing flow-induced vibrations in a uniform flow. Mar. Struct. 61, 326–342.

Li, T., Ishihara, T., 2021. Numerical study on vortex-induced vibration of circular cylinder with two-degree-of-freedom and geometrical nonlinear system. J. Fluid Struct. 107, 103415.

Liu, G., Li, H., Qiu, Z., Leng, D., Li, Z., Li, W., 2020. A mini review of recent progress on vortex-induced vibrations of marine risers. Ocean. Eng. 195, 106704.

Lu, Y., Luo, Q., Liao, Y., Xu, W., 2022. Vortex-induced vibration fatigue damage prediction method for flexible cylinders based on RBF neural network. Ocean. Eng. 254, 111344.

Lu, Y., Liu, Z., Zhang, Q., Xu, W., Xu, Z., 2023. Flow-induced vibration (FIV) fatigue damage characteristics of two unequal-diameter flexible cylinders in a staggered arrangement. Ocean. Eng. 283, 114947.

Ma, Y., Xu, W., Liu, B., 2019. Dynamic response of three long flexible cylinders subjected to FIV in an equilateral-triangular configuration. Ocean Eng 183, 187–207.

Ma, Y., Luan, Y., Xu, W., 2020. Hydrodynamic features of three equally spaced, long flexible cylinders undergoing flow-induced vibration. Eur. J. Mech. B-Fluids 79, 386–400.

Ma, Y., Xu, W., Ai, H., Wang, Y., Jia, K., 2021. The effect of time-varying axial tension on VIV suppression for a flexible cylinder attached with helical strakes. Ocean. Eng. 241, 109981.

Ma, Y., Xu, W., Pang, T., Wang, Q., Lai, J., 2020. Dynamic characteristics of a slender flexible cylinder excited by concomitant vortex-induced vibration and time-varying axial tension. J. Sound Vib. 485, 115524.

Mentzelopoulos, A.P., del Águila Ferrandis, J., Rudy, S., Sapsis, T., Triantafyllou, M.S., Fan, D., 2022. Data-driven prediction and study of vortex induced vibrations by leveraging hydrodynamic coefficient databases learned from sparse sensors. Ocean. Eng. 266, 112833.

Resvanis, T.L., Vandiver, J.K., Fu, S.X., Asme, 2015. Ramp tests: a novel approach to VIV model testing of flexible cylinders using continuously varying towing speeds. In: 34th ASME International Conference on Ocean, Offshore and Arctic Engineering (OMAE2015). CANADA, St John's.

Sanaati, B., Kato, N., 2012. A study on the effects of axial stiffness and pre-tension on VIV dynamics of a flexible cylinder in uniform cross-flow. Appl. Ocean Res. 37, 198–210.

Song, L., Fu, S., Cao, J., Ma, L., Wu, J., 2016. An investigation into the hydrodynamics of a flexible riser undergoing vortex-induced vibration. J. Fluid Struct. 63, 325–350.

Triantafyllou, M.S., Bourguet, R., Dahl, J., Modarres-Sadeghi, Y., 2016. Vortex-induced vibrations. In: Dhanak, Manhar R., Xiros, N.I. (Eds.), Springer Handbook of Ocean Engineering. Springer International Publishing, Cham, pp. 819–850.

Trim, A.D., Braaten, H., Lie, H., Tognarelli, M.A., 2005. Experimental investigation of vortex-induced vibration of long marine risers. J. Fluid Struct. 21 (3), 335–361.

Vandiver, J.K., Ma, L., Rao, Z., 2018. Revealing the effects of damping on the flow-induced vibration of flexible cylinders. J. Sound Vib. 433, 29–54.

Wang, J., Fu, S., Baarholm, R., Wu, J., Larsen, C.M., 2014. Fatigue damage of a steel catenary riser from vortex-induced vibration caused by vessel motions. Mar. Struct. 39, 131–156.

Wang, Y., Gao, D., Fang, J., 2015. Coupled dynamic analysis of deepwater drilling riser under combined forcing and parametric excitation. J. Nat. Gas Sci. Eng. 27, 1739–1747.

Wu, Z., Dong, H., Ma, H., Ni, P., Xiao, Y., Mei, G., 2021. A stochastic analysis approach for marine riser's cross-flow/in-line VIV under heave-induced parametric vibration. Ships Offshore Struct. 17 (5), 952–972.

Xu, W., Ma, Y., Luo, H., Luan, Y., 2017. Identification and characteristics of hydrodynamic coefficients for a flexible cylinder undergoing vortex-induced vibration. Chin. J. Theor. Appl. Mech. 49 (4), 818–827.

Xu, W., Qin, W., Gao, X., 2018. Experimental study on streamwise vortex-induced vibration of a flexible, slender cylinder. Appl. Sci. 8 (2), 311.

Xu, W., Li, Y., Jia, K., Yu, Y., 2020a. FIV induced fatigue damage of two side-by-side flexible cylinders in a uniform flow. Ocean. Eng. 217, 107898.

Xu, W., Li, Y., Ma, W., Liang, K., Yu, Y., 2020b. Effects of spacing ratio on the FIV fatigue damage characteristics of a pair of tandem flexible cylinders. Appl. Ocean Res. 102, 102299.

Xu, W., Qin, W., Yu, Y., 2020. Flow-induced vibration of two identical long flexible cylinders in a staggered arrangement. Int. J. Mech. Sci. 180, 105637.

Xu, W., Zhang, Q., Lai, J., Wang, Q., Yu, Y., 2020c. Flow-induced vibration of two staggered flexible cylinders with unequal diameters. Ocean. Eng. 211, 107523.

Xu, W., Zhang, S., Liu, B., Wang, E., Bai, Y., 2018. An experimental study on flow-induced vibration of three and four side-by-side long flexible cylinders. Ocean Eng 169, 492–510.

Xu, W., Zhang, S., Ma, Y., Liu, B., 2021a. Fluid forces acting on three and four long side-by-side flexible cylinders undergoing flow-induced vibration (FIV). Mar. Struct. 75, 102877.

Xu, W., Zhang, S., Ma, Y., Liu, B., Wang, J., 2021b. A study on the FIV hydrodynamic force coefficients of two staggered flexible cylinders via an inverse method. Ocean Eng 219, 108272.

Xu, W., Zhang, Q., Ma, Y., Wang, Y., He, C., Lai, J., 2022. Hydrodynamic characteristics of two side-by-side flexible cylinders with different diameters experiencing flow-induced vibration. Ocean Eng 243, 110199.

Yang, H., Xiao, F., 2014. Instability analyses of a top-tensioned riser under combined vortex and multi-frequency parametric excitations. Ocean. Eng. 81, 12–28.

Yuan, Y., Xue, H., Tang, W., Liu, J., 2021. Fatigue analysis of vortex-induced vibration for marine risers with top-end platform motion excitations. In: Okada, T., Suzuki, K., Kawamura, Y. (Eds.), Practical Design of Ships and Other Floating Structures. Springer Singapore, Singapore, pp. 639–656.

Zhang, X., Gou, R., Yang, W., Chang, X., 2018. Vortex-induced vibration dynamics of a flexible fluid-conveying marine riser subjected to axial harmonic tension. J. Braz. Soc. Mech. Sci. Eng. 40 (8), 365.

Zhang, Y., Gui, Q., Yang, Y., Li, W., 2022. The instability and response studies of a top-tensioned riser under parametric excitations using the differential quadrature method. Mathematics 10 (8), 1331.